Application of geophysical methods for the investigation of the large gravitational mass movement of Séchilienne, France

O. Meric, S. Garambois, D. Jongmans, M. Wathelet, J.L Chatelain, and J.M. Vengeon

Abstract: Several geophysical techniques (electromagnetic profiling, electrical tomography, seismic refraction tomography, and spontaneous potential and seismic noise measurement) were applied in the investigation of the large gravitational mass movement of Séchilienne. France. The aim of this study was to test the ability of these methods to characterize and delineate the rock mass affected by this complex movement in mica schists, whose lateral and vertical limits are still uncertain. A major observation of this study is that all the zones strongly deformed (previously and at present) by the movement are characterized by high electrical resistivity values (>3 kΩ·m), in contrast to the undisturbed mass, which exhibits resistivity values between a few hundred and 1 kΩ·m. As shown by the surface observations and the seismic results, this resistivity increase is due to a high degree of fracturing associated with the creation of air-filled voids inside the mass. Other geophysical techniques were tested along a horizontal transect through the movement, and an outstanding coherency appeared between the geophysical anomalies and the displacement rate curve. These preliminary results illustrate the benefits of combined geophysical techniques for characterizing the rock mass involved in the movement. Results also suggest that monitoring the evolution of the rock mass movement with time-lapse geophysical surveys could be beneficial.

Key words: gravitational movement, geophysical methods, Séchilienne.

Résumé : Plusieurs techniques géophysiques (profil électromagnétique, tomographie électrique, tomographie sismique et potentiel spontané et bruit de fond sismique) ont été appliquées pour la reconnaissance du grand mouvement de terrain de Séchilienne (France) situé dans des micaschistes. L'objectif de cette étude était de tester ces méthodes géophysiques afin de caractériser et de délimiter la masse de roche affectée par ce mouvement complexe dont la limite latérale reste incertaine. L'étude a montré que toutes les zones très déformées (encore actuellement et dans le passé) par le mouvement sont caractérisées par de fortes valeurs de résistivité électrique (supérieure à 3 kΩ·m), tandis que dans la zone non perturbée les valeurs de résistivité sont de quelques centaines de Ω·m à 1 kΩ·m. Comme le montrent les observations de surface et les profils de tomographie sismique, cette augmentation de résistivité est due à une fracturation importante associée à la création de vides remplis d'air au sein du massif. Les techniques électromagnétiques, PS et de mesure de bruit ont été testées le long d'un profil transversal recoupant le mouvement. Une corrélation remarquable est obtenue entre les anomalies géophysiques et le taux de déplacement. Ces résultats préliminaires soulignent l'intérêt de combiner les méthodes géophysiques pour caractériser la masse de roche impliquée dans le mouvement et pour déterminer l'évolution du mouvement par un suivi temporel des paramètres géophysiques.

Mots clés : mouvement gravitaire, méthodes géophysiques, Séchilienne.

Introduction

Various types of failure, such as toppling, sagging, and translational or rotational sliding (Hutchinson 1988), may occur during large gravitational movements, which are common in the crystalline formations of mountain ranges. In some cases, one of these mechanisms can evolve into a catastrophic failure and into a long-runout avalanche, such as the recent rockslides of Valpola, Italy, in 1987 (Azzoni et al. 1992) and Randa, Switzerland, in 1991 (Noverraz and Bonnard 1991) or the prehistoric events of Köfels, Austria, and Langtang, Nepal (Erismann and Abele 2001). In con-

Received 30 March 2004. Accepted 1 March 2005. Published on the NRC Research Press Web site at http://cgj.nrc.ca on 30 August 2005.

O. Meric[1]. Laboratoire interdisciplinaire de recherche impliquant la géologie et la mécanique, B.P. 53–38041 Grenoble CEDEX 9, France; and Societé Alpine de géotechnique Z.I. de Mayencin, B.P. 17–38610 Gières, France.
S. Garambois, D. Jongmans, M. Wathelet, and J.M. Vengeon. Laboratoire interdisciplinaire de recherche impliquant la géologie et la mécanique, B.P. 53–38041 Grenoble CEDEX 9, France.
J.L Chatelain. Laboratoire de géophysique interne et tectonophysique; and Institut de recherche et de développement Grenoble, B.P. 53–38041 Grenoble CEDEX 9, France.

[1]Corresponding author (e-mail: Ombeline.Meric@ujf-grenoble.fr).

 doi: 10.1139/T05-034

trast, large, slow rockslides with signs of self-stabilizing movement have also been observed; an example is the La Clapière rockslide in gneiss (Follacci et al. 1988). The different failure processes are mainly governed by the rock properties and the characteristics of the discontinuities (foliation, schistosity, faults, and fractures) affecting the rock mass (Antoine et al. 1994; Glastonbury and Douglas 2000). From the study of two large-scale field examples and numerical modelling, Nichol et al. (2002) recently distinguished two alternative modes of toppling in rock slopes: ductile flexural toppling in weak rocks (schist and phyllite) with a single dominant joint; and brittle block toppling in strong rocks (granite) with well-developed cross-joints. These researchers concluded that the brittle process can lead to rock avalanches, whereas the other one exhibits slow deformations without a catastrophic event. Rockslide failures can, however, be highly complex and involve several deformation mechanisms relating to geological variations, weathering, influence of groundwater conditions, and the presence of faults and several fracture sets.

In the Alps, most of the large gravitational movements were probably initiated or reactivated after the retreat of glaciers (Noverraz 1996) some 10 000 – 15 000 years ago. The movements have evolved at very different rates, depending on the initial geological and topographic characteristics, as well as on the other factors contributing to lower stability (influence of water, toe erosion, earthquake ground motions, and climatic cycles). The instability process progresses through periods of stabilization and reactivation and leads to slope failure after decades or centuries.

Forecasting the failure characteristics of a rockslide remains a difficult problem, mainly because of the difficulty of obtaining reliable and representative information on the geometry, rheology, and kinematics of the unstable slope (Crosta and Agliardi 2003; Moser 2002; Noverraz 1996). This lack of information can only be mitigated by the observation, investigation, and monitoring of numerous sites over long periods. In the last 10 years, innovative techniques have emerged in geodesy for measuring ground displacements on the surface (global positioning systems; synthetic aperture radar interferometry) and in applied geophysics for imaging the subsurface. In parallel, 2D and 3D numerical modelling methods have been developed that can better simulate the complexity of the mechanisms. However, because of the large uncertainties in input parameters, the use of numerical modelling is mainly limited to back analysis and to the understanding of the significant factors leading to failure. In combination, all these investigative techniques and computational methods offer researchers the opportunity to get a better insight into the deformation mechanisms of rock slopes (Brückl 2001; Havenith et al. 2003).

In this study, we used geophysical prospecting methods to investigate the large gravitational mass movement of Séchilienne (the French Alps). In the past, except for some seismic reflection or refraction experiments (e.g., Bogoslovsky and Ogilvy 1977; McCann and Forster 1989), geophysical methods were rarely applied to such slides, particularly in rocky conditions. This is probably partly due to the difficulties of deploying geophysical sensors in rocky ground and taking measurements on steep slopes. Recently, several studies using different geophysical techniques were performed in mountainous areas on large slides (Bruno and Marillier 2000; Brückl 2001; Havenith et al. 2002; Supper and Römer 2003; Lapenna et al. 2003). Advantages of geophysical methods are that they are fairly flexible, they give information on the inside of the mass, and they can investigate a large volume of rock. The main drawbacks are the decreasing resolution with depth, the need for calibration, and the indirect information (geophysical parameters) they yield. Some of the measured parameters (seismic velocity, for instance) can, however, be correlated with mechanical properties, such as the degree of fracturing (Sharma 1997). Recent developments in geophysical prospecting make it possible to generate images of the subsurface distribution of geophysical properties by inverting the acquired data (Reynolds 1997). In particular, electrical tomography (ET) and seismic tomography (ST) are now standard methods (Jongmans et al. 2000; Havenith et al. 2002; Lapenna et al. 2003) that can contribute useful information, in addition to high-resolution seismic reflection surveys (Bruno and Marillier 2000). However, Musil et al. (2002) recently showed that in shallow low-velocity and heterogeneous layers (rock glaciers), seismic reflection failed to map the bedrock surface. The main factor contributing to this failure was the unexpected low-frequency signals returned by the subsurface as a result of the anelastic attenuation, scattering, and low-pass filter effect of the heterogeneous shallow layer. In contrast, the *P*-wave refraction tomography technique provided reliable information on the structure of the rock glacier.

The aim of this study was to test the applicability of a variety of geophysical techniques (electromagnetic (EM) profiling, ET, ST, and spontaneous potential (SP) and seismic noise (SN) measurements) in the investigation of a large movement in crystalline formations. The seismic reflection technique was discarded in the first stage, because of the high heterogeneity of the slope and the difficulty of continuously deploying geophones in such an environment.

The Séchilienne mass movement

The Séchilienne movement, located in the French Alps, near Grenoble, is affecting the right south-facing bank of the Romanche River (Fig. 1). The slope consists mainly of mica schists with interbedded quartz–feldspar-rich layers, whose thickness can reach a few metres. These rocks were affected by the Hercynian and Alpine orogenies, resulting in a near-vertical foliation that is at right angles to the valley, except in the upper part of the slope, where it is folded with an axis inclined 30° northward (see Fig. 3). In the lower part of the hill, at an elevation of 330–950 m above sea level (a.s.l.), the slope is about 40°–50° (Fig. 2), but it decreases to 20° between 950 and 1100 m a.s.l. (Mont Sec area). Near the crest, a scarp that is a >20 m high and several hundred metres long (Fig. 3) reveals an upper subsidence. The nonfreshness of the scarp shows that this movement is old; it was probably initiated or reactivated after the retreat of glaciers. Because of the tectonic history, the mass is cut by several faults (F1–F4, Fig. 3) and three sets of near-vertical fractures (Pothérat and Alfonsi 2001). The main fracture family, running N70°E, delimits vertical slices in the rock mass and is clearly distinguished by depressions, several hundred metres long, in the morphology; these depressions are associated

Fig. 1. Location and topographical map of the Séchilienne movement. Ellipse delineates the most active zone. Circle indicates the location of the survey gallery.

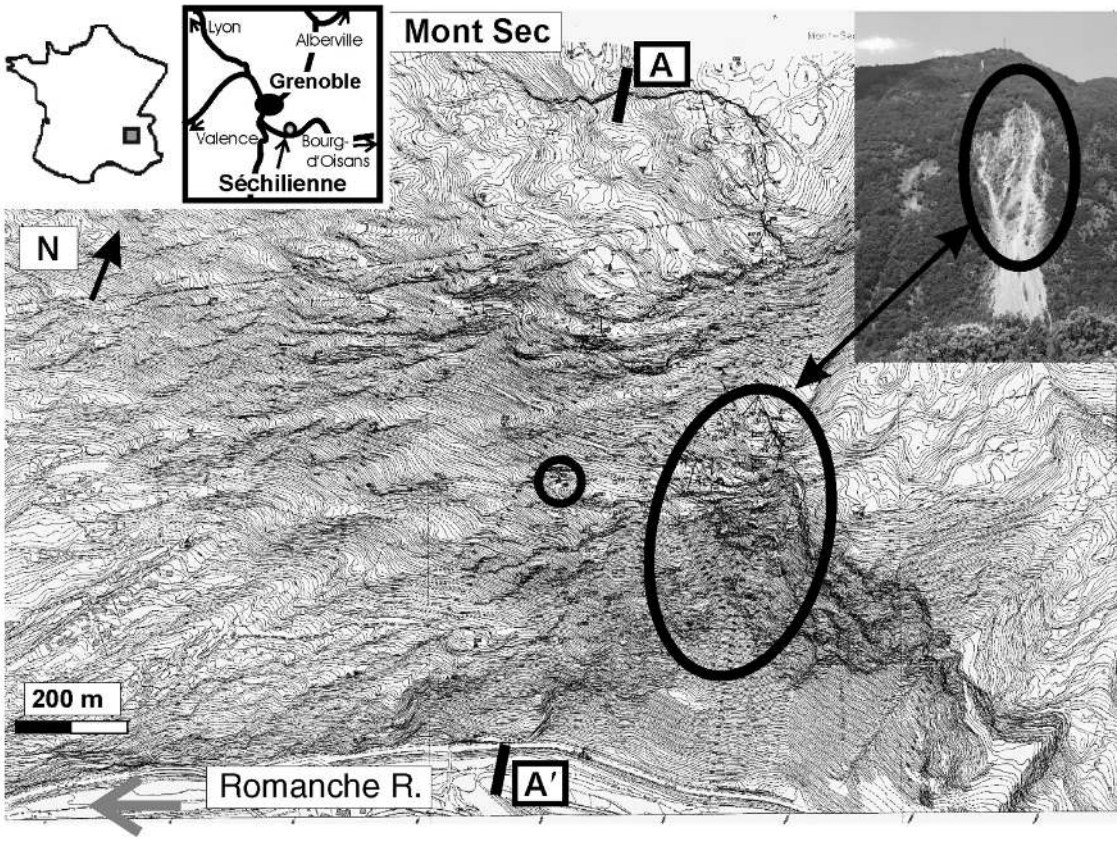

Fig. 2. Cross section (labelled A–A′ in Fig. 1) through the Séchilienne movement, with the location of the survey gallery and the kinematic model deduced from the displacement measurements within the gallery (after Vengeon 1998).

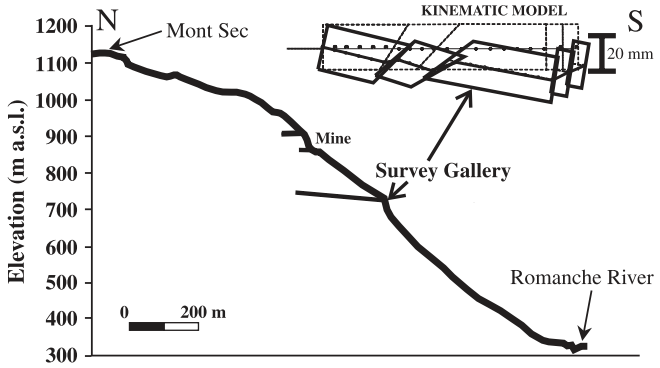

with north-facing scarps several metres high (Figs. 1 and 3) (Vengeon 1998). Some of the depressions are 20 m wide, attesting to the lengthy duration of the gravity-induced processes. At a late tectonic stage, the rock mass was cut by metallic sulphur veins, which were worked at different levels during the 19th and 20th centuries (Durville et al. 2004).

The part of the slope that exhibits more signs of current instability (high-motion zone, Fig. 1) is in the middle of the hill, at an elevation of 600–900 m a.s.l., and involves a rock volume estimated from geometric constraints to be about 3×10^6 m^3 (Giraud et al. 1990). This area has been extensively instrumented since 1988 (Evrard et al. 1990; Duranthon et al. 2003); the measured displacements are globally oriented in a south-southeast direction (Fig. 3), perpendicular to the strike of the main fractures, and dip downhill between 10° and 20°. The displacement rate in the high-motion zone varies from 15 cm/year to 1 m/year and regularly decreases to the north and to the west. In 1993–1994, a 240 m long gallery was excavated at 710 m in a zone to the west of the high-motion zone and characterized by a displacement rate of about 5 cm/year (see Figs. 1 and 2). Displacement measurements and observations inside the gallery showed a succession of rigid moving blocks delimited by highly fractured zones parallel to the main fracture set. These blocks exhibit differential normal faulting movement, as shown by the kinematic model presented in Fig. 2. Unfortunately, the gallery did not reach the sound rock, and the existence of a sliding surface is still an open question. On the basis of structural data, numerical modelling of the rock mass was performed with the discrete element method (Vengeon 1998; Pothérat and Alfonsi 2001), which modelled the main field observations. These results suggest that the movement at Séchilienne is controlled by the principal discontinuities, where the mass breaks into blocks, and includes toppling and local sliding, evolving from progressive damage to a potential large slide of unknown characteristics.

Isotopic and hydrochemical methods were used to investigate groundwater movement inside the Séchilienne slope (Vengeon 1998; Guglielmi et al. 2002). This analysis showed the existence of a deep saturated zone, which extends into

Fig. 3. Topographical map with the main geological structures and displacement rate affecting the Séchilienne hill. The high-motion zone is shaded in grey. This map also shows the location of the geophysical profiles: electromagnetic (EM), electrical tomography (ET), and seismic tomography (ST). Three geophysical measurement methods, EM, seismic noise (SN), and spontaneous potential (SP), were used along the EM2 profile. Finally, this map outlines the main electrical contrasts found by the survey and their relation to morphological features. Electrical contrasts are represented by boxes, the resistive part of which is darker: points f and g are on the Mont Sec scarp; points h and j are on the eastern limits of the movement; point k marks a limit inside the movement that delineates the most active part; points b and i are located on faults F2 and F4, respectively; and points a, c, d, and e are deduced from geophysical prospecting.

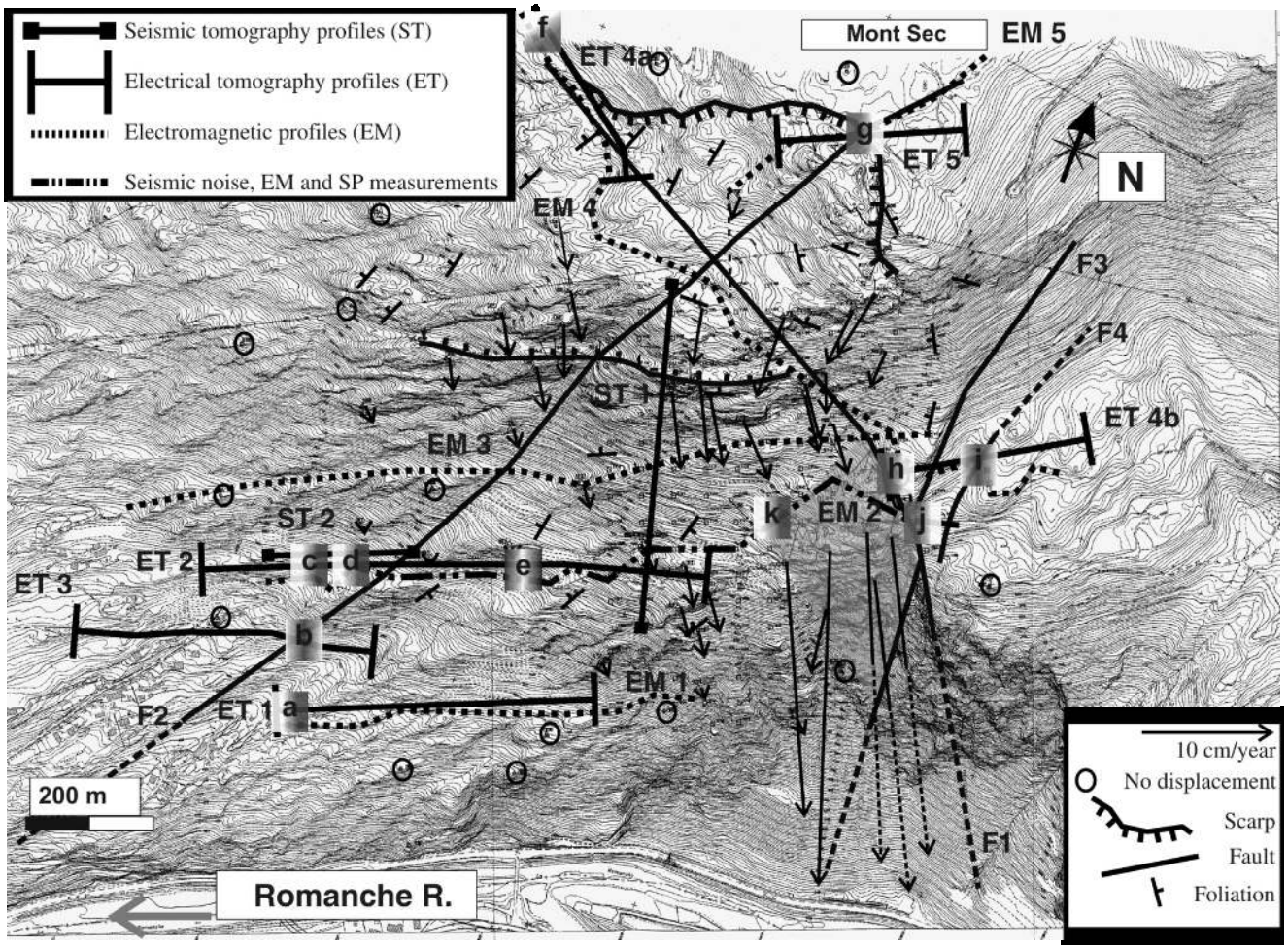

the fractured metamorphic bedrock, with a probable 100 m thick vadose zone above. With intensive rainfall and long-time water recharge, this vadose zone could be saturated for a short time, increasing the displacement rate.

The data available at Séchilienne have led some authors to propose that the hill could be affected by a massive movement, delineated to the east by the high-motion zone and to the north by the Mont Sec scarp. No western limit is clearly visible in the topography, and the thickness of this potentially moving mass is unknown. Consequently, the volume estimations for a rock avalanche scenario are highly variable and poorly constrained, ranging from 3×10^6 to 20×10^6 m^3 (Giraud et al. 1990; Antoine et al. 1994) inside a total, slowly moving mass of (50–100) $\times 10^6$ m^3. It is noticeable that a rockfall of more than 3×10^6 m^3 can generate a secondary hazard, flooding, by damming the valley (upstream, during filling of the reservoir created by the dam; downstream, in case of dam failure). Furthermore, the presence of an active seismic strike-slip fault (Thouvenot et al. 2003) has recently been pointed out in the vicinity of the landslide, indicating the possibility of an earthquake trigger for a rockfall.

Geophysical investigation

Five geophysical methods (EM profiling, ET, ST, and SP and SN measurements) were applied to delineate the mass affected by the movement and to find possible relations between geophysical parameters and zones of rock deformation. The principles of the first four methods can be found in Reynolds (1997). Geophysical tests are being used more often now for engineering site characterization (Foti and Butcher 2004). In a rock mass, geophysical properties (primarily electrical resistivity and seismic velocity in our study) can vary with the nature of the geologic formation and the degree of fracturing and weathering, as well as with the presence of water. For example, an increase in the degree

Fig. 4. Electromagnetic profiles EM1–EM5: points f and g are on the Mont Sec scarp; points h and j are on the eastern limits of the movement; point k marks a limit inside the movement that delineates the most active part; point i is located on fault F4; and points a, c, and d are deduced from geophysical prospecting.

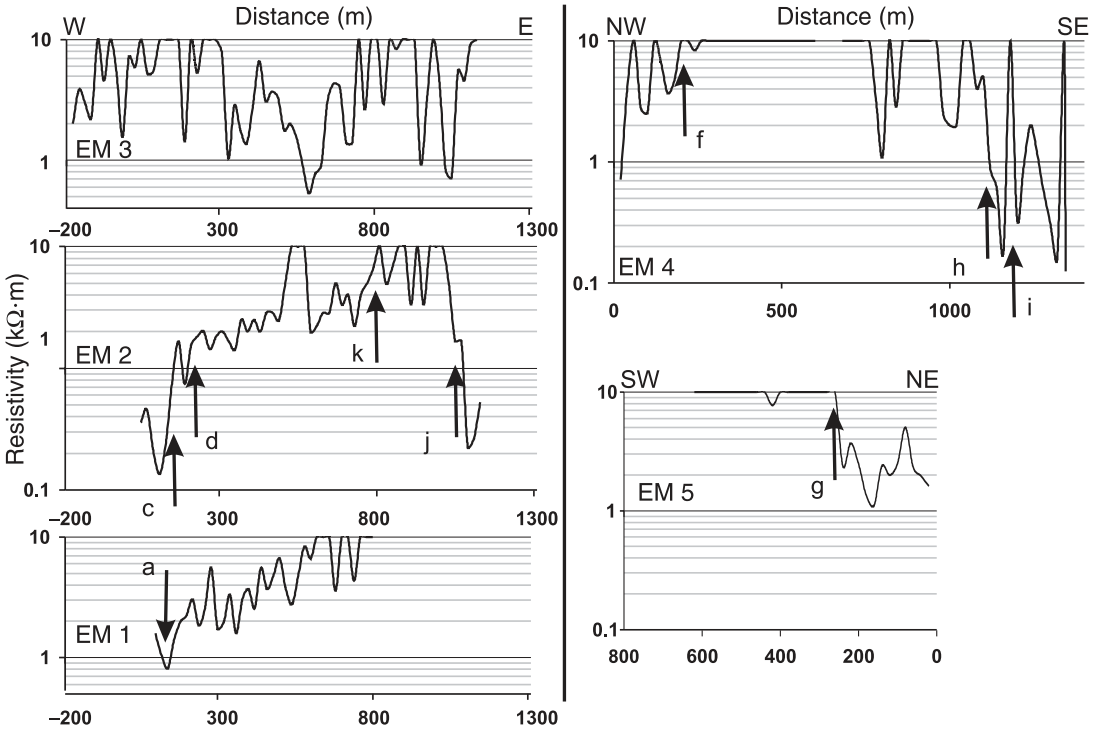

of fracturing leads to a decrease in *P*-wave velocity and variations in electrical resistivity, depending on the water content. In a dry context, increased fracturing will lead to increased electrical resistivity.

Electromagnetic profiling

As a first step, EM profiles were recorded with a ground conductivity meter (EM34, Geonics Ltd., Mississauga, Ont.) at different locations on the hill. This method, which yields a single apparent electrical resistivity value at each measurement location, was favoured because it does not require that electrodes be driven into the ground. The EM measurements were performed with horizontal loops, an intercoil separation of 20 m, and a measurement interval of 20 m. Penetration depth ranged from 4 to 30 m with this configuration, with a maximum contribution from approximately 8 m. EM measurements were taken along five transects (labelled EM1–EM5 in Fig. 3) across the movement zone; the resulting curves are displayed in Fig. 4. Vertical dipole measurements show that the apparent resistivity values range from 0.2 to >10 kΩ·m, which is the limit of the device. Profile EM5 crosses the Mont Sec scarp, the location of which is shown by a resistivity increase from about 2 kΩ·m to > 10 kΩ·m in the subsiding zone (at point g, Fig. 4). Profile EM4 also starts above the Mont Sec scarp, crosses the area of rock movement, and ends in the undisturbed zone, east of fault F4 (Figs. 3 and 4). Apparent resistivity values, which are between 0.5 kΩ·m and a few kΩ·m at both ends of the profile, dramatically increase (>10 kΩ·m) in the deformed zone defined between the Mont Sec scarp and fault F1 (at points f and h, Fig. 4). A local resistivity increase (at point i, Fig. 4) was also observed where fault F4 crosses the profile. The three other profiles, EM1, EM2, and EM3, orientated approximately west-southwest–east-northeast (Fig. 3), were recorded at elevations of 460–560, 540–840, and 590–870 m a.s.l., respectively. To the west, the resistivity measured along profile EM2 regularly increases from <1 kΩ·m (at points c and d, Fig. 4) to >10 kΩ·m in the high-motion zone, whose limits are at points k and j. At the limit with the undisturbed rock, the resistivity strongly decreases to <1 kΩ·m (at point j, Fig. 4). Profile EM1, which is shorter, exhibits a similar increase from the west to the western limit of the high-motion zone, which is impossible to cross. In contrast, resistivity values at the western end of profile EM3 do not show a clear decrease. The transect was made along a major depression corresponding to a fracture zone, which probably influences the resistivity values. Resistivity values of <1 kΩ·m are locally observed in the middle of the profile. The results from the EM transects suggest that the strongly fractured zones are well correlated with high resistivity values and can be distinguished from the undisturbed mass, which is characterized by apparent resistivity values of <1 kΩ·m close to the surface.

Electrical tomography

We tried to understand the observed variations in apparent resistivity more quantitatively and at greater depths by recording six ET profiles along specific lines, whose length varied from 320 to 750 m. The electrical data were processed with the algorithm developed by Loke and Barker (1996). Unlike EM profiling, ET involve inversion of direct-current resistivity field data to produce models of the distribution of the ground's electrical resistivity directly under the survey line. Resulting images show real electrical resistivity

Fig. 5. Electrical images ET1–ET5. Vertical arrows and labels are the same as in Fig. 4. The RMS values after inversion are 5% for ET1, 5% for ET2, 7.5% for ET3, 3% for ET4a, 5% for ET4b, and 2% (ET5).

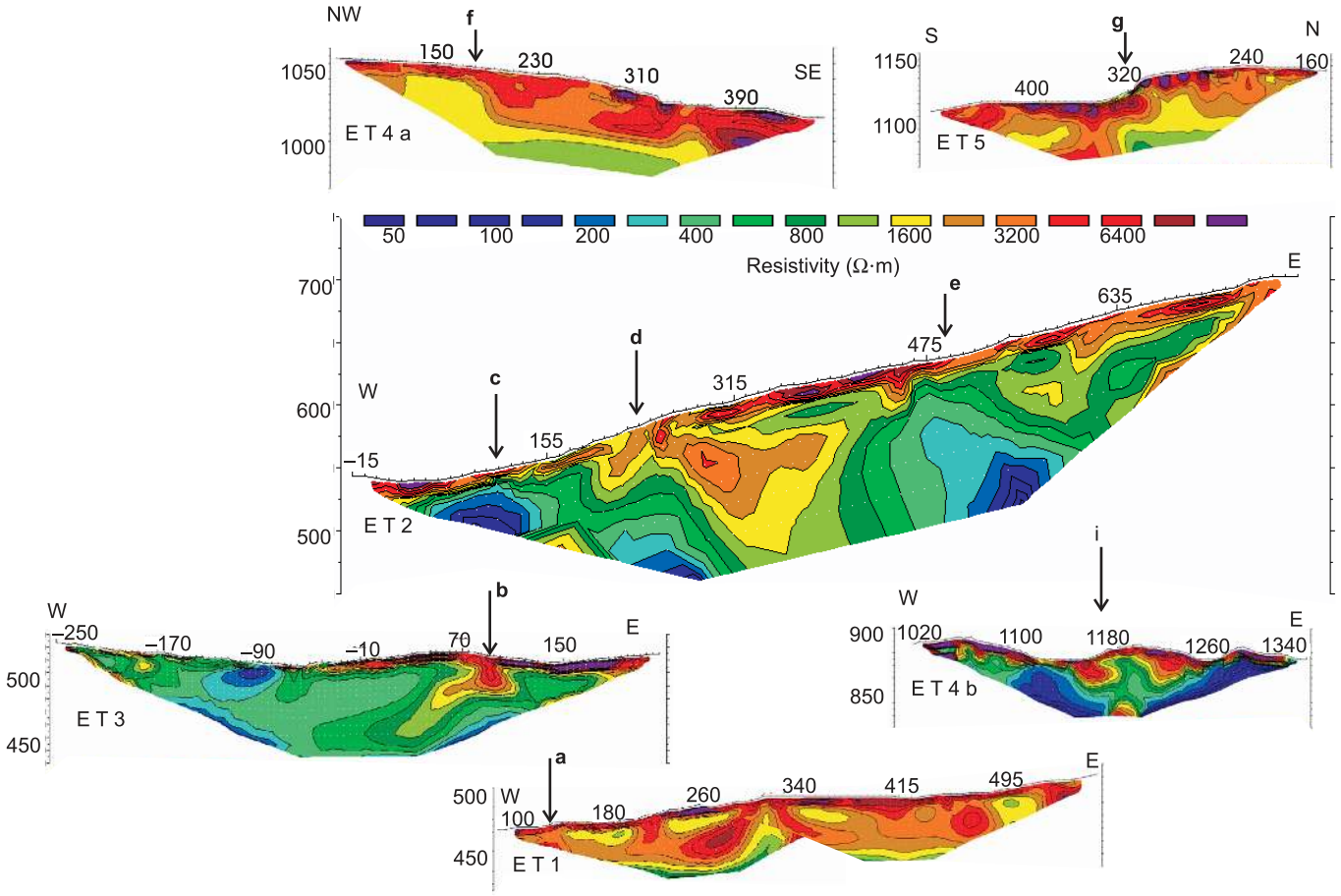

values, and the vertical axis represents the true depth under the profile line. The derived models are smoothed, owing to the methodology, and the final deduced solution must not be considered as unique, because of the sparsity of field data. Nevertheless, the inversion reliably provides estimates of the broader scale variations within the ground. Figure 5 presents six ET sections (ET1–ET4a, ET4b, and ET5; see Fig. 3). Models shown in Fig. 5 were obtained by inversion, which yielded root mean square (RMS) values of 5%, implying that each model was reliably able to reproduce its corresponding dataset. Profile ET4b was recorded in the eastern unaffected zone, where mica schists outcrop. Below a resistive layer of rock debris a few metres thick, the bedrock exhibits a resistivity of 50–800 Ω·m, with a vertical resistive zone (at point i) already shown on EM4 and corresponding to the presence of a fault (F4 in Fig. 3). Profile ET5 was recorded at the top of the movement across the Mont Sec scarp (Fig. 3; point g in Fig. 5), where the transect EM5 was carried out. Below a highly resistive surficial layer of debris and glacial deposits, a few metres thick, the resistivity values are globally higher than in ET4b, with a lateral resistivity increase below the Mont Sec scarp, from about 800 Ω·m to 3 kΩ·m in the settled zone (at point g). This latter zone is also characterized by its thicker surficial resistive layer. These results explain the lateral variation of the EM data across the scarp. Another electrical profile (ET4a) was recorded along EM4 at the western end of the Mont Sec scarp. This electrical profile also shows a lateral resistivity contrast (at point f), with increased thickness of the resistive layer to the south. Three other ET profiles (ET1–ET3) were recorded to the west, parallel to profiles EM1 and EM2 (Fig. 3). The first one (ET2), which is 750 m long and reaches a penetration depth of >100 m, exhibits strong lateral resistivity contrasts (at points c, d, and e). The first two of these (points c and d) correspond to an eastward resistivity increase, which is consistent with the results of the EM2 profile. In particular, the first contrast (at point c), from 200 to >1 kΩ·m, fits with the strong resistivity rise noticed along the EM2 profile, whereas the second one corresponds to the trace of fault F2. The third electrical contrast corresponds to the presence of a more conductive zone at depth. Profile ET3 is located farther west than the other profiles. Below a surficial resistive layer, the corresponding image exhibits resistivity values of <750 Ω·m in the western part of the profile, with a lateral resistivity increase (at point b) that is consistent with the location of fault F2.

Finally, the ET1 profile shows relatively high resistivity values (usually >1 kΩ·m in the upper 30 m), with a general increase of the average resistivity of the surficial layers to the east, consistent with the data from EM1. An important feature of this image is the vertical decrease in resistivity with depth below 30 m, where values as low as 800 Ω·m are

Fig. 6. Comparison between the electrical (*a*) and seismic (*b*) tomography sections ET2 and ST2: points c and d are at the limits deduced from geophysical prospecting. The RMS values after inversion are 5% for ET2 and 2% for ST2.

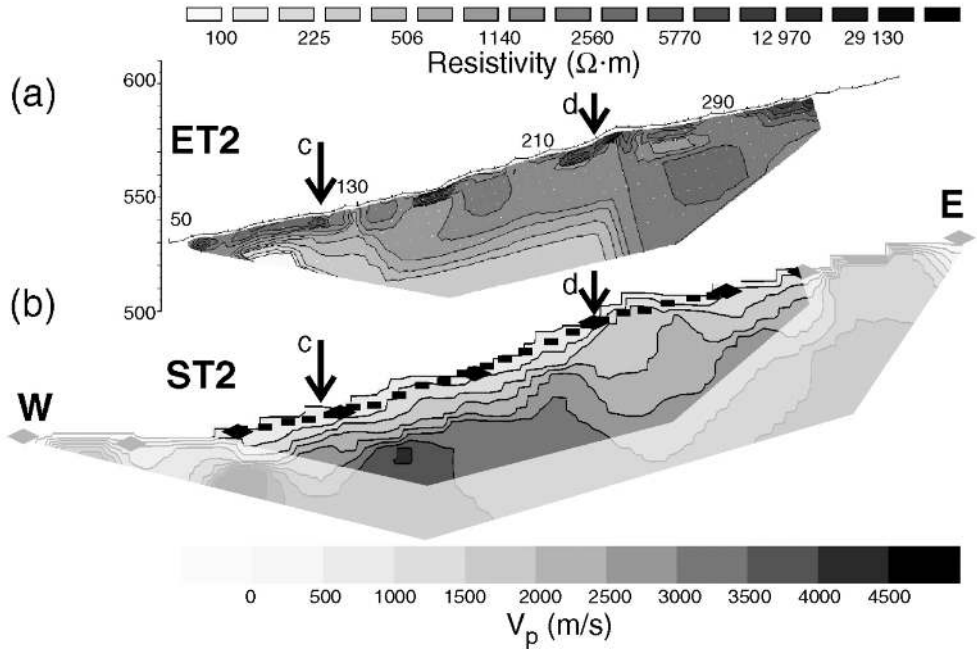

reached. This result, which suggests the presence of sound bedrock at that depth, was checked by using another inversion technique, DCIP2D (UBC–GIF 2001), which is based on subspace methods (Oldenburg et al. 1993). The obtained image (not shown here) also exhibits a low-resistivity zone (about 800 Ω·m) below 35 m depth. When the technique proposed by Oldenburg and Li (1999) was applied, the depth of investigation was estimated to be about 45 m, supporting the presence of sound bedrock below 30 or 35 m.

The EM and electrical profiles show a significant increase in electrical resistivity values when entering the zone affected by the gravitational movement, both at the two limits of the high-motion zone (at points k and j, Fig. 5) and across the Mont Sec scarp. This global electrical resistivity rise probably results from the presence of air-filled voids induced by the deformation. Some local lateral resistivity variations have, however, been observed within the movement area, which probably result from differences in the fracturing degree and (or) in the rock types. Also, the measurements in the supposedly undisturbed zone show a large resistivity range, from 100 Ω·m to the east of the movement to >1 kΩ·m in the Mont Sec area, which might, however, be affected by fracturing above the upper main scarp. Finally, the vertical resistivity variations seem to indicate the presence of undisturbed bedrock approximately 30 m below ET1 and >100 m below the central part of ET2.

Seismic tomography

The ST technique, which consists of inverting first-arrival times to get an image of *P*-wave velocity distribution in the ground, is applied, in engineering geology, between boreholes and at the surface (e.g., Lanz et al. 1998; Jongmans et al. 2000). For this study two long seismic profiles (300 and 650 m) were recorded, and the first-arrival times were inverted by the simultaneous iterative reconstruction technique (Dines and Lyttle 1979). The strong eastward resistivity increase (at points c and d, Fig. 5), observed on both the EM2 and the ET2 profiles, was investigated with a 300 m long seismic refraction profile. Ten shots were recorded by 24 geophones 10 m apart, and the *P*-wave first-arrival times were inverted. The resulting seismic image is compared with the electrical one in Fig. 6. The measured seismic velocities, V_p, range from 500 m/s at the surface (weathered layer, rock debris) to 4000 m/s (sound bedrock) at depth. The seismic image also shows lateral variations, and the previously described eastward resistivity increase, from 200 Ω·m to 1 k Ω·m, is clearly correlated with a seismic velocity decrease, from 3500 m/s to about 2000 m/s (at point d). These results provide strong evidence that the resistivity decrease is caused by a higher degree of fracturing, which also lowered the seismic velocity values. For the 650 m long seismic profile, we made use of the 240 m long survey gallery to perform ST between the slope surface and the gallery. Forty-eight geophones, 10–15 m apart, recorded the signals generated by 24 explosions (see Figs. 4 and 8). The seismic image obtained after inversion of the travel-time values (with RMS error of 1%) is presented in Fig. 7. The robustness of the image was tested with different initial models. As in the 300 m profile, the major features are the large range of *P*-wave seismic velocities, whose values range between 500 and 5000 m/s, and the presence of strong lateral velocity gradients. Considering that the volume investigated is fairly homogeneous rock (mica schists), these two features highlight the strong fracturing and weathering, whose intensity not only is depth dependent but also varies laterally. No systematic surficially damaged zone overlying the sound bedrock has been detected, at least not down to 100 m depth. These results, showing the juxtaposition of near-vertical highly fractured zones and little deformed blocks, are consistent with geological field observations and motion measurements

Fig. 7. Seismic tomography profile ST1 between the survey gallery and the slope. RMS = 1%.

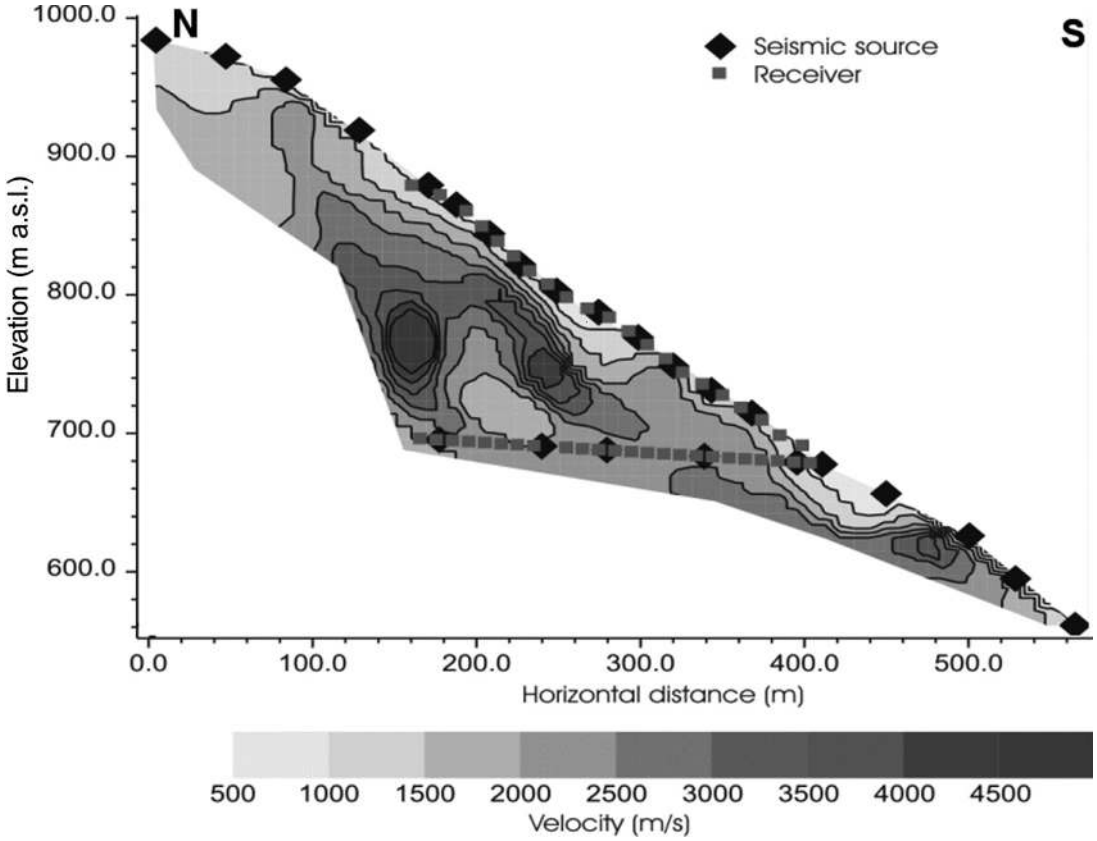

at the surface and in the gallery, as well as with the geological model used for discrete numerical simulations (Vengeon 1998; Pothérat and Alfonsi 2001). This seismic image suggests that the survey gallery was driven into a lower velocity zone that is too wide to have resulted from the decompression around the gallery. This survey, which involved measurements between the surface and the underground gallery, used an unusual configuration that provided high-quality, continuous information on the rock mass inside the moving massif.

Spontaneous potential and seismic noise measurements

Finally, two other techniques, SP and SN measurements, were tested. The SP method measures differences in natural electrical potentials, which can be produced by electrochemical, mineral, and electrokinetic effects (Reynolds 1997). In recent decades, SP measurements have been regularly used for detecting groundwater flow in landslides (Bogoslovsky and Ogilvy 1977; Giano et al. 2000; Bruno and Marillier 2000). In our study, SP data, as well as SN data, were acquired along the EM2 profile, which crosses the movement zone. In Fig. 8 are plotted the SP values (Fig. 8*a*), profile EM2 (Fig. 8*b*), the noise measurements (Fig. 8*c*), and the mean displacement rate during the last 2 years. The measured SP values (Fig. 8*a*) range from –100 to 350 mV. The SP anomaly is positive across the movement and becomes negative at both ends. The shapes of the SP and displacement rate curves are similar, showing two maxima at the same location. The stronger SP positive anomaly is observed over the high-motion zone. Similar results were also obtained on the Boup landslide (Bruno and Marillier 2000), where SP data showed a positive anomaly over the landslide body, particularly in the vicinity of the boundary between the landslide and the stable ground. At this stage, it is difficult to determine which SP source produces these large anomalies. Repeated measurements were made along the same profile at three different dates over a period of 7 months. They show very stable behaviour with time across the movement (Fig. 8*a*). These large, stable positive and negative anomalies could be generated by the geological structure of the movement (fracturing, lead–zinc and quartz veins) and (or) a permanent, deep main water flow nearly parallel to the surface. However, Fig. 8*a* also displays local SP variations with time, particularly outside the mass movement, where the profile crosses faults F3 at 1220 m a.s.l. and F4 at 1360 m a.s.l. (see Fig. 3). These variations could be electrokinetically generated by fluid flow changes inside these major discontinuities.

SN measurements are used in earthquake engineering for estimating site effects (Bard 1998) or in exploration for mapping soft deposits (e.g., Delgado et al. 2000). In our study, measurements of ambient vibration were made every 50 m along the same profile (EM2) with a 5 s sensor. Figure 8*c* displays the behaviour of the mean spectral amplitude computed between 0.25 and 35 Hz along this line. As the vibrations were measured at different periods, they were all normalized with a reference station. Dramatic variations (from 1 to 10) of the noise energy were observed. The striking feature is that the spectral amplitude values are higher in the same zone as the SP and apparent resistivity curves, and

Fig. 8. Geophysical anomalies along electromagnetic profile EM2. (*a*) Spontaneous potential data measured on three dates (black curve, December 2003; light grey curve, March 2004; dark grey curve, June 2004). (*b*) Electromagnetic profile EM2. (*c*) Spectral amplitude of the seismic noise computed between 0.5 and 30 Hz. (*d*) Displacement rate. Points c and d are at the limits deduced from geophysical measurements; points k and j are morphological limits (k marks a limit inside the movement that delineates the most active part; and j is at the eastern limit of the movement).

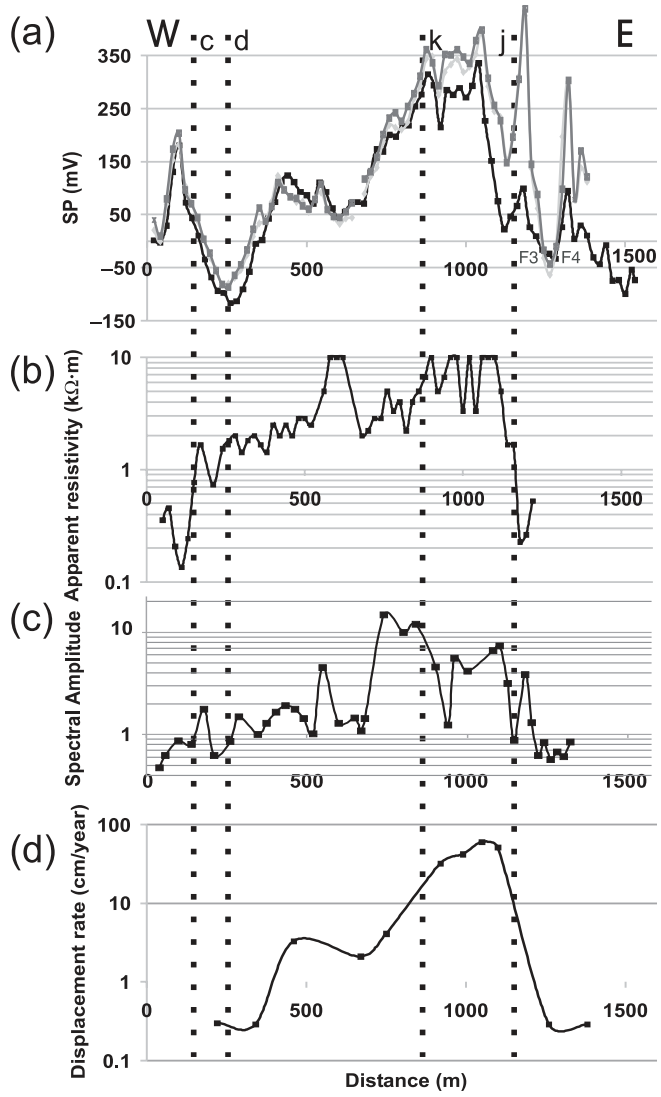

they significantly decrease at both ends of the profile. A possible explanation for these results is the decrease in *P*-wave and *S*-wave velocities with rock deformation. This phenomenon generates a ground motion amplification effect, whose magnitude increases with the seismic impedance contrast between the deformed zone and the underlying bedrock (Bard and Bouchon 1990).

Discussion and conclusions

Five geophysical techniques (EM profiling, ET, ST, and SP and SN measurements) were applied on the large gravitational movement of Séchilienne, with the aim of characterizing and delineating the mass affected by the movement. Because of the difficulty of performing tests on steep slopes, the number of geophysical profiles is limited, and the results presented here allow only preliminary conclusions to be drawn. A major outcome of this study is that all zones exhibiting signs of present-time or previous movements (collapse, toppling, sliding) are characterized by high electrical resistivity values (>3 kΩ·m), compared with the undisturbed zones (between a few hundred and 800 Ω·m). Figure 3 shows the location of the main electrical contrasts pointed out by the survey. This relation between electrical resistivity and gravitational deformation was particularly well demonstrated in the Mont Sec subsiding area (at points f and g, Fig. 3) and at the two limits of the present-time high-motion zone (at points k and j). The consistency between the geophysical parameters and the displacement rates was also shown along east–west-oriented profile EM2. It is reasonable to assume that the present relative rates of movement at Séchilienne reflect the total relative movement that has occurred since movement began along this profile. The very good agreement between the two curves (Figs. 8*c* and 8*b*) and the inverse relation between electrical resistivity and *P*-wave velocity (Fig. 6) support the interpretation that resistivity variations along the profile are mainly related to the degree of fracturing. The resistivity increase corresponds to a *P*-wave velocity decrease, both of which can result from fracturing and the creation of voids that are not filled with water over a depth of a several tens of metres. Most remarkable is the similarity in the overall shape of the four curves of Fig. 8: all exhibit an asymmetric bell shape with a maximum across the high-motion zone. Our interpretation is that this area, which now experiences the highest displacement rates, exhibits the highest resistivity values because of the presence of voids, is probably the place of deep preferential groundwater flow (SP data), and has the lowest V_s and V_p values (highest noise spectral amplitudes). The eastern limit of the movement is clearly indicated by a sharp geophysical contrast (at points h and j, Fig. 3), as all the curves show a regular decrease to the west. However, the negative–positive SP anomaly, the local resistivity and seismic gradients, and to a lesser extent, the noise amplitude all suggest that the western limit of the zone affected by the movement could be between points c and d along ET2 and around point a along ET1 (Figs. 3 and 8). At these sites all the measured geophysical data have approximately the same values as those from the eastern unaffected zone. As observed on the curves of Fig. 8 and in other data presented above, strong lateral variations are present along the geophysical profiles. These variations in geophysical parameters probably result from the numerous fractures and faults of tectonic origin that affected the massif before the movement. However, these low-strength discontinuities have without doubt controlled the action of the forces of gravity, resulting in a heterogeneous deformation pattern juxtaposing near-vertical, highly fractured zones and little deformed blocks, as observed in the gallery and as shown by the seismic and electrical images.

The limit of the movement at depth was a major focus of this study. Although most of the geophysical images show prominent horizontal variations, which probably mask the vertical ones, some indications of characteristics at depth

were given. At its western limit, electrical image ET2 (Fig. 5) nicely shows the deepening of the sound bedrock top, which is located at a minimum of 40 m depth across point d, if we consider the 800 Ω·m isoline as this boundary. Similarly, the depth to bedrock can be estimated as being at about 30 m below ET1, which is the only electrical image showing a clear resistivity decrease with depth. Below the Mont Sec scarp, section ET5 gives a depth of >40 m for the sound bedrock. Finally, image ST1 and profile ET2 apparently did not detect the sound bedrock within 100 m. All these results indicate that the Séchilienne movement is deep seated, with heterogeneous deformation, as locally shown by the investigation gallery.

The geophysical campaign on the Séchilienne movement tested different techniques and has brought new information on the characteristics of the deformed zone. In future, the first objective will be to delineate the zone affected by the movement to the northwest, where the boundary is quite uncertain. An effort will also be made to more quantitatively interpret the results of SP and SN measurements. Other fast and innovative techniques, such as the transient electromagnetic method (Reynolds 1997) and noise array measurements (Wathelet et al. 2004), will also be tested in an effort to detect the undisturbed bedrock top. Finally, the outstanding coherence between geophysical anomalies and displacement rate data highlights the potential for using time-lapse geophysical techniques as a component of a monitoring system; this has been initiated on other movements (Supper and Römer 2003).

Acknowledgements

This work was partially supported by the Pôle grenoblois des risques naturels through funding from the General Council of Isère (France). We thank all the numerous and enthusiastic participants in the field campaigns, the Centre d'études techniques de l'équipement of Lyon for providing the displacement measurements, and P. Desvarreux (SAGE Co.) for fruitful discussions. Our special thanks go to Frederic Nguyen for his help with estimating the depth of investigation along ET profiles. The Laboratoire interdisciplinaire de recherche impliquant la géologie et la mécanique is part of the French Risques naturels et vulnérabilité des ouvrages network.

References

Antoine, P., Giraud, A., Evrard, H., and Rochet, L. 1994. A huge slope movement at Séchilienne, Isère, France. Landslide News, **8**: 15–18.

Azzoni, A., Chiesa, S., Frassoni, A., and Govi, M. 1992. The Valpola landslide. Engineering Geology, **33**: 59–70.

Bard, P.-Y. 1998. Microtremor measurements: a tool for site effect estimation? *In* Proceedings of the 2nd International Symposium on the Effects of Surface Geology on Seismic Motion, Yokohama, Japan, 1–3 December 1998. *Edited by* K. Iribura, K. Kudo, H. Okada, and T. Sasatani. A.A. Balkema, Rotterdam, The Netherlands, pp. 1251–1279.

Bard, P.-Y., and Bouchon, M. 1980. The seismic response of sediment-filled valleys. Part 1. The case of incident SH waves. Bulletin of the Seismological Society of America, **70**: 1263–1286.

Bogoslovsky, V.A., and Ogilvy, A.A. 1977. Geophysical methods for the investigation of landslides. Geophysics, **42**: 562–571.

Brückl, E.P. 2001. Cause–effect models of large landslides. Natural Hazards, **23**: 291–314.

Bruno, F., and Marillier, F. 2000. Test of high-resolution seismic reflection and other geophysical techniques on the Boup landslide in the Swiss Alps. Surveys in Geophysics, **21**: 333–348.

Crosta, G.B., and Agliardi, F. 2003. Failure forecast for large rock slides by surface displacement measurements. Canadian Geotechnical. Journal, **40**: 176–191.

Delgado, J., Lopez Casado, C., Estevez, A., Giner, J., Cuenca, A., and Molina, S. 2000. Mapping soft soils in the Segura River valley (SE Spain): a case of study of microtremors as an exploration tool. Journal of Applied Geophysics, **45**: 19–32.

Dines, K., and Lyttle, J. 1979. Computerized geophysical tomography. Proceedings of the Institute of Electrical and Electronics Engineers, **67**: 1065–1073.

Duranthon, J.-P., Effendiantz, L., Mémier, M., and Prévitali, I. 2003. Apport des méthodes topographiques et topométriques au suivi du versant rocheux instable des ruines de Séchilienne. *XYZ* revue de l'AFT, **94**: 31–38.

Durville, J.L., Effendiantz, L., and Potherat, P. 2004. The Séchilienne landslide. *In* Identification and mitigation of large landslide risks in Europe. A.A. Balkema, Rotterdam, The Netherlands. p. 317.

Erismann, T.H., and Abele, G. 2001. Dynamics of rockslides and rockfalls, Springer-Verlag, New York.

Evrard, H., Gouin, T., Benoit, A., and Duranthon, J.-P. 1990. Risques majeurs d'éboulements en masse : point de surveillance du site. Bulletin de liaison des laboratoires des ponts et chaussées, **165**: 7–16.

Follacci, J.-P., Guardia, P., and Ivaldi, J.-P. 1988. Le glissement de La Clapière dans son cadre géodynamique. *In* Proceedings of the 5th International Symposium on Landslides, Lausanne, Switzerland. pp. 1323–1327.

Foti, S., and Butcher, A.P. 2004. General report: geophysical methods applied to geotechnical engineering. *In* Geotechnical and Geophysical Site Characterization: Proceedings of the 2nd International Conference on Site Characterization, ISC-2, Porto, Portugal, 19–22 September 2004. *Edited by* A. Viana da Fonseca amd P.W. Mayne. Millpress Science Publishers. Vol. 1, pp. 409–418.

Giano, S.I., Lapenna, V., Piscitelli, S., and Schiatarella, M. 2000. Electrical imaging and self-potential surveys to study the geological setting of the Quaternary slope deposits in the Agri high valley (southern Italy). Annali di Geofisica, **43**: 409–419.

Giraud, A., Rochet, L., and Antoine, P. 1990. Processes of slope failure in crystallophyllian formations. Engineering Geology, **29**: 241–253.

Glastonbury, J., and Douglas, K. 2000. Catastrophic rock slope failures: observed characteristics and behaviour. *In* GeoEng2000: An International Conference on Geotechnical and Geological Engineering, Melbourne, Australia, 19–24 November 2000. Technomic Publishing, Lancaster, Pa. Vol. 2.

Guglielmi, Y., Vengeon, J.M., Bertrand, C., Mudry, J., Follacci, J.-P., and Giraud, A. 2002. Hydrogeochemistry: an investigation tool to evaluate infiltration into large moving rock masses (case study of La Clapière and Séchilienne alpine landslides). Bulletin of Engineering Geology and the Environment, **61**: 311–324.

Havenith, H.B., Jongmans, D., Faccioli, E., Abdrakhmatov, K., and Bard, P.-Y. 2002. Site effects analysis around the seismically induced Ananevo rockslide, Kyrgyzstan. Bulletin of the Seismological Society of America, **92**: 3190–3209.

Havenith, H.B., Strom, A., Calvetti, F., and Jongmans, D. 2003. Seismic triggering of landslides. Part B: Simulation of dynamic failure processes. Natural Hazards and Earth System Sciences, **3**: 663–682.

Hutchinson, J.N. 1988. General report: morphological and geotechnical parameters of landslides in relation to geology and hydrogeology. *In* Proceedings of the 5th International Symposium on Landslides, Lausanne, Switzerland. *Edited by* C. Bonnard. A.A. Balkema, Rotterdam, The Netherlands, Vol. 1, pp. 3–35.

Jongmans, D., Hemroulle, P., Demanet, D., Renardy, F., and Vanbrabant, Y. 2000. Application of 2D electrical and seismic tomography techniques for investigating landslides. European Journal of Environmental and Engineering Geophysics, **5**: 75–89.

Lanz, E., Maurer, H., and Green, A.G. 1998. Refraction tomography over a buried waste disposal site. Geophysics, **63**: 1414–1433.

Lapenna, V., Lorenzo, P., Perrone, A., Piscitelli, S., Sdao, F., and Rizzo, E. 2003. High-resolution geoelectrical tomographies in the study of Giarrossa landslide (southern Italy). Bulletin of Engineering Geology and the Environment, **62**: 259–268.

Loke, M.H., and Barker, R.D. 1996. Rapid least-squares inversion of apparent resistivity pseudosections by a quasi-Newton method. Geophysical Prospecting, **44**: 131–152.

McCann, D.M., and Forster, A. 1989. Reconnaissance geophysical methods in landslide investigations. Engineering Geology, **29**: 59–78.

Moser, M. 2002. Geotechnical aspects of landslides in the Alps. *In* Proceedings of the 1st European Conference on Landslides, Prague, Czech Republic, 25–28 November 2002. *Edited by* J. Rybar, J. Stemberk, and P. Wagner. A.A. Balkema, Lisse, The Netherlands, pp. 355–361.

Musil, M., Maurer, H., Green, A.G., Horstmeyer, H., Nitsche, F.O., Vonder Muhl, D., and Springman, S. 2002. Shallow seismic surveying of an alpine rock glacier. Geophysics, **67**: 1701–1710.

Nichol, S.L., Hungr, O., and Evans, S.G. 2002. Large-scale brittle and ductile toppling of rock slopes. Canadian Geotechnical Journal, **39**: 773–788.

Noverraz, F. 1996. Sagging or deep-seated creep: fiction or reality? *In* Proceedings of the 7th Symposium on Landslides, Trondheim, Norway, 17–21 June 1996. *Edited by* K. Senneset. A.A. Balkema, Rotterdam, The Netherlands, pp. 821–828.

Noverraz, F., and Bonnard, C. 1991. L'écroulement rocheux de Randa, près de Zermatt. *In* Landslides: Proceedings of the 6th International Symposium on Landslides, Christchurch, N.Z.. Ashgate, pp.165–170.

Oldenburg, D.W., and Li, Y. 1999. Estimating depth of investigation in DC resistivity and IP surveys. Geophysics, **64**: 403–416.

Oldenburg, D.W., McGillivray, P.R., and Ellis, R.G. 1993. Generalized subspace methods for large-scale inverse problems. Geophysical Journal International, **114**: 12–20.

Pothérat, P., and Alfonsi, P. 2001. Les mouvements de versant de Séchilienne (Isère). Revue française de géotechnique, **95–96**: 117–131.

Reynolds, J.M. 1997. An introduction to applied and environmental geophysics. John Wiley & Sons, New York.

Sharma, P.V. 1997. Environmental and engineering geophysics. Cambridge University Press, Cambridge, U.K.

Supper, R., and Römer, A. 2003. New achievements in developing a high speed geoelectrical monitoring system for landslide monitoring. *In* Proceedings of the 9th Meeting of Environmental and Engineering Geophysics, Prague, Czech Republic. O-004.

Thouvenot, F., Fréchet, J., Jenatton, L., and Gamond, J.-F. 2003. The Belledonne border fault: identification of an active seismic strike-slip fault in the western Alps. Geophysical Journal International, **155**: 174–192.

UBC–GIF. 2001. DCIP2D: a program library for forward modelling and inversion of DC resistivity and induced polarization data over 2D structures. Version 3.2. Developed under the consortium research project Joint/Cooperative Inversion of Geophysical and Geological Data, The University of British Columbia's Geophysical Inversion Facility, Department of Earth and Ocean Sciences, Vancouver, B.C.

Vengeon, J-M. 1998. Déformation et rupture des versants en terrain métamorphique anisotrope : apport de l'étude des ruines de Séchilienne. Ph.D. thesis, Université Joseph Fourier, Grenoble.

Wathelet, M., Jongmans, D., and Ohrnberger, M. 2004. Surface wave inversion using a direct search algorithm and its application to ambient vibration measurements. Near Surface Geophysics, **2**: 211–221.